


FULL PAPER

Concurrent effects of wafer temperature and oxygen fraction on cryogenic silicon etching with SF₆/O₂ plasmas

Stefan Tinck¹  | Thomas Tillocher² | Violeta Georgieva¹ | Rémi Dussart² | Erik Neyts¹ | Annemie Bogaerts¹

¹ Research Group PLASMANT, Department of Chemistry, University of Antwerp, Universiteitsplein 1, Antwerp, Belgium

² GREMI, CNRS/Université d'Orléans, Orléans, France

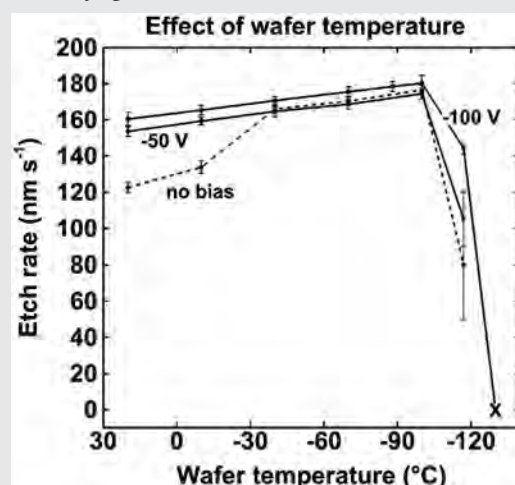
Correspondence

Dr. Stefan Tinck, Research Group PLASMANT, Department of Chemistry, University of Antwerp, Universiteitsplein 1, Antwerp B-2610, Belgium.
Email: stefan.tinck@uantwerpen.be

Funding information

Fonds Wetenschappelijk Onderzoek (FWO), Grant number: 0880.212.840; Hercules Foundation; Flemish Government (Department EWI); University of Antwerp

Cryogenic plasma etching is a promising technique for high-control wafer development with limited plasma induced damage. Cryogenic wafer temperatures effectively reduce surface damage during etching, but the fundamental mechanism is not well understood. In this study, the influences of wafer temperature, gas mixture and substrate bias on the (cryogenic) etch rates of Si with SF₆/O₂ inductively coupled plasmas are experimentally and computationally investigated. The etch rates are measured in situ with double-point reflectometry and a hybrid computational Monte Carlo – fluid model is applied to calculate plasma properties. This work allows the reader to obtain a better insight in the effects of wafer temperature on the etch rate and to find operating conditions for successful anisotropic (cryo)etching.



KEYWORDS

cryogenic, etching, plasma, SF₆, silicon

1 | INTRODUCTION

Porous low-*k* materials have gained increasing interest in the microelectronics industry during the past decade due to their promising properties for advanced interconnect technologies in microchip manufacturing.^[1] The main problem with etching these porous materials is plasma induced damage (PID). During etching with PID, the material is significantly damaged by ion bombardment, and especially by diffusion of reactive species (e.g., F atoms) into the material, effectively increasing its *k*-value and thus degrading the quality of the isolating porous material.

PID can be limited by two techniques that recently became popular and involve cooling the wafer to cryogenic temperatures (i.e., near $-100\text{ }^{\circ}\text{C}$): (i) filling of the pores prior to etching so that diffusion through the pores of undesired species is avoided^[2] and (ii) etching with SF₆/O₂ so that an oxifluoride passivation layer is formed on the surface of the pores that also reduces diffusion through the material. Both techniques can also be applied simultaneously.^[3]

During SF₆/O₂ cryogenic deep reactive ion etching (DRIE), first proposed in 1988 by Tachi et al.,^[4] a SiF_xO_y passivation layer is formed, which desorbs naturally when the wafer is brought back to room temperature, leaving a clean

trench with no scalloping.^[5] However, the underlying mechanisms of how the SiF_xO_y passivation layer is formed and automatically desorbs afterwards are not yet fully understood.^[6] A topical review by Dussart et al.^[6] covers the latest advances in cryoetching, ranging from the origin of cryoetching to today's technologies.

Silicon etching with a fluorine-containing gas, like CF_4 , SF_6 , C_4F_8 , etc., has been around for decades and is a well known process to anisotropically etch silicon. Etch rates of Si and SiO_2 in SF_6/O_2 plasmas have been studied by d'Agostino and Flamm as a function of gas mixture at 1 Torr.^[7] They found that there is a broad chemical analogy with CF_4/O_2 plasmas. The plasma etching of silicon and silicon dioxide in CF_4/O_2 mixtures has also been studied before by Mogab et al. as a function of feed-gas composition using a number of different diagnostics.^[8]

Furthermore, Bartha et al. studied etching of Si with SF_6 , using a Helicon type plasma source. In contrast to the current understanding of low temperature etching, they obtained isotropic etch profiles even at temperatures below -120°C . On the other hand, anisotropic etch profiles were obtained when they added O_2 to the SF_6 plasma.^[9] The same conclusion was drawn by D'Emic et al. who developed a new magnetron ion etching process to etch $50\ \mu\text{m}$ deep trenches into silicon. Their optimized SF_6/O_2 gas mixture results in a nearly vertical etch profile with a vertical to horizontal etch rate ratio of 9:4.^[10] Also Campo et al. investigated reactive ion etching of Si (and Ge) in SF_6/O_2 plasmas.^[11]

The effects of reactive ion etching of Si in SF_6 and SF_6/O_2 plasmas on the Si–Si wafer bonding properties were also investigated by Reiche et al. They found that wafers etched with SF_6 showed bonding behavior similar to hydrophobic samples while addition of O_2 caused the Si surfaces to become hydrophilic.^[12]

There is a fair amount of experimental work on cryogenic etching. A cryogenic SF_6/O_2 plasma process has been used by Craciun et al. to investigate the etching of deep holes in Si wafers. The influences of crystallography and aspect ratio on the holes have been explored. It was found that wafer temperature played a crucial role during the etching process in controlling the anisotropy created due to crystal orientation dependent etching.^[13] Moreover, Dussart et al. investigated the passivation mechanisms of Si trenches involved in SF_6/O_2 cryogenic etching.^[14] They showed that the passivating layer is removed during the increase of the wafer temperature leading to a very clean surface of the sidewalls after processing but numerical studies are limited. The same group wrote the topical review on cryogenic etching.^[6]

There are some computational studies of SF_6/O_2 plasmas but they do not explicitly refer to cryoetching. Blauw et al.^[15] investigated the kinetics of SF_6/O_2 anisotropic Si etching with a Monte Carlo (MC) surface model and experiments. Their modeling work was limited to surface interactions without

gas phase plasma calculations. Marcos et al.^[16] also performed MC etch profile simulations with SF_6/O_2 . They varied the F atom sticking coefficient and compared the calculated profile with experimental results, to determine the overall sticking probability for F atoms during trench or hole etching.

Furthermore, Pateau et al. performed global model calculations to investigate the plasma kinetics for different fractions of oxygen in an $\text{SF}_6/\text{O}_2/\text{Ar}$ ICP.^[17] Also, Hamaoka et al. performed simulations on a SF_6/O_2 mixture, but for a capacitively coupled plasma focusing on deep reactive ion etching of MEMS.^[18] Moreover, we recently did a computational study on cryogenic etching of Si with pure SF_6 plasma, specifically focused on cryogenic etching, but not including a passivating gas like O_2 .^[19]

Ryan and Plumb previously developed a model to describe the SF_6/O_2 plasma chemistry and the etching of Si with these plasmas,^[20] while Anderson et al. made time-dependent Boltzmann electron distribution calculations at constant power and pressure in a SF_6/O_2 plasma with a varying oxygen fraction. Their simulations help to explain the increasing anisotropic etch character with greater oxygen dilution of SF_6 .^[21]

In recent years, not only low- k dielectric cryoetching but also silicon cryoetching has gained increasing interest. The primary difficulty with SF_6/O_2 cryogenic DRIE is the high sensitivity to the oxygen content and the substrate temperature. The success of an anisotropic etch process with minimal PID depends strongly on the exact balance between etching and passivation layer formation on the sidewalls. Especially the degree of passivation is influenced by the O_2 fraction in the SF_6/O_2 mixture, in combination with a specific (cryogenic) wafer temperature. The goal of this work is therefore to investigate how the O_2 content and the wafer temperature work together, establishing the overall resulting etch and passivation rates, and how we can tune these process parameters for successful anisotropic etching.

The experimental and computational details including the SF_6/O_2 reaction set are presented in Section 2 while the results are discussed in Section 3.

2 | EXPERIMENTAL

2.1 | Experimental details

An Alcatel 601E ICP reactor is used to etch Si wafers of 15 cm diameter with an SF_6/O_2 ICP.^[22] A three-dimensional sketch of the reactor geometry is shown in Figure 1.

The SF_6/O_2 mixture is fed from the top nozzle and the plasma is sustained by the ICP coil surrounding the 20 cm diameter alumina tube powered by an RF power supply at 13.56 MHz. Underneath the source there is a 40 cm diameter diffusion chamber with the wafer at the center bottom. The

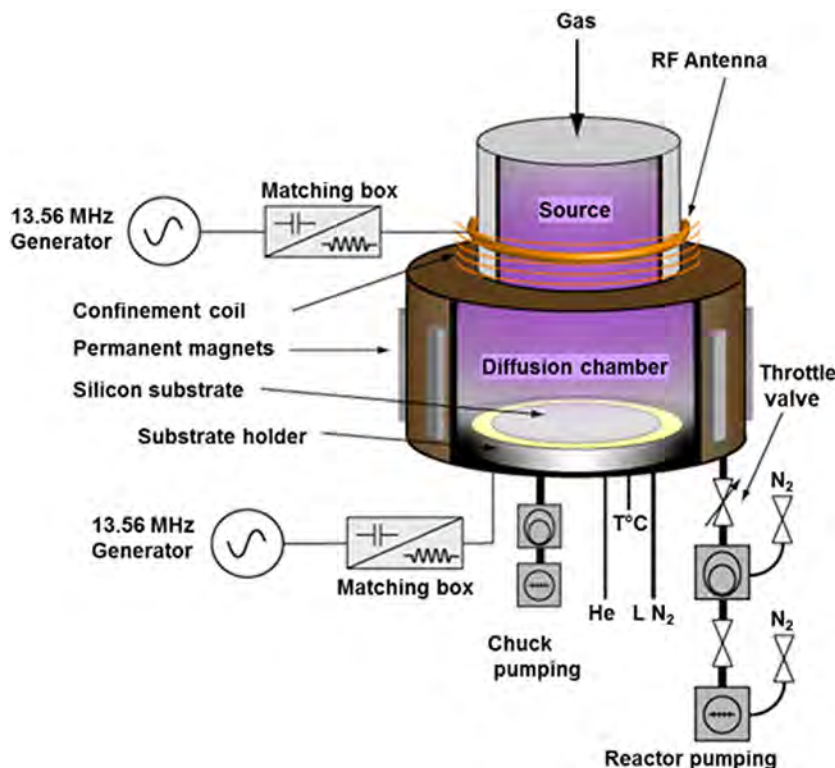


FIGURE 1 Illustration of the ICP reactor used for the experiments

wafer temperature is controlled from the bottom with liquid nitrogen and heating elements. The chamber is surrounded by permanent magnets as shown in the sketch, but these magnets were not activated for the experiments concerning this work.

Square Si wafer samples (1 cm^2), with a SiO_2 mask for etching $500 \mu\text{m}$ holes, were glued on a carrier wafer covered by SiO_2 . The etch rate is measured in situ with double-point reflectometry, which consists of a 650 nm laser diode from which two separate spots can be positioned at different spots on the wafer: usually a point on the mask and one inside a hole. The interacting phase shift between the two reflected beams is recorded to obtain the etch rate.

2.2 | Computational details

The hybrid plasma equipment model (HPEM), that is, a two-dimensional plasma model developed by Kushner, is applied to understand the plasma properties.^[23] It consists of (i) a module for calculating the electromagnetic fields by solving Maxwell's equations; (ii) a module for addressing the electron properties by solving the electron energy equation; and (iii) a fluid module for all heavy species. With these modules, the SF_6/O_2 plasma can be self-consistently described. A more detailed description of the model can be found elsewhere.^[23] The species included in the model are listed in Table 1. Tests have been performed with and without excited states for O_2 . The considered states for O_2 are: one ground state level and two electronic excited levels with thresholds of 8.40 and 10.00 eV ; for these three states, one

rotational excitation and two vibrational excitations are included with thresholds of 0.02 , 0.19 , and 0.38 eV . This yields a total of nine electron impact excitation reactions for O_2 . However, it could be concluded that these excited states of O_2 could be neglected because they did not significantly affect the final results of the SF_6/O_2 simulations.

Concerning wall collisions, we defined a simplified reaction set where we allow each species to reflect from the walls as its neutral ground state counterpart except for electrons who are lost permanently at the walls. We do allow F atoms to recombine to F_2 at the wafer and walls with a probability of 20% .

The reaction set that defines the SF_6/O_2 plasma chemistry is presented in Tables 2 and 3, where Table 2 lists the electron impact reactions and Table 3 the reactions between heavy particles. The labels listed in Table 2 correspond to the cross sections shown in Figure 2A-D. The reaction set consists of a set for pure O_2 combined with a set for pure SF_6 , including cross-product ion-ion neutralizations. It also includes several SO_xF_y reaction cross-products, adopted from Hamaoka et al.^[18] and Rauf et al.^[24]

The electronically excited species F^* and O^* both comprise two different electronic states with different threshold energies, that is, F^* (12.70 and 12.99 eV) and O^* (1.97 and 4.19 eV). For the sake of completeness of the reaction set, we opt to include all possible combinations of ion-ion neutralizations as these reactions typically have high rates. However, most of these rates are not known but can be predicted by a formula constructed by Shuman et al.^[25]

$$k = 3.3 \times 10^{-7} \mu^{-0.5} E_{\text{BE}}^{-0.24}$$

where k is the rate coefficient (in $\text{cm}^3 \text{ s}^{-1}$), μ is the reduced mass of the colliding species (in Da) and E_{BE} is the absolute value of the electron binding energy of the anion (in eV). It must be noted that this formula is suitable for collisions of polyatomic ions. For collisions of two monoatomic ions, the rate coefficient predicted by this formula is typically about one order of magnitude too high. In these cases, we have used

TABLE 1 List of heavy species included in the model

Neutral ground state species	SF_6 , SF_5 , SF_4 , SF_3 , SF_2 , SF , S , F , F_2 , O_2 , O , SOF , SOF_2 , SOF_3 , SOF_4 , SO_2 , SO_2F_2
Positive ions	SF_3^+ , SF_4^+ , SF_5^+ , SF_6^+ , SF^+ , S^+ , F^+ , F_2^+ , O_2^+ , O^+
Negative ions	SF_6^- , SF_5^- , SF_4^- , SF_3^- , SF_2^- , F^- , O^-
Electronically excited species	F^* (12.70 eV and 12.99 eV), O^* (1.97 eV and 4.19 eV)

TABLE 2 Electron impact reactions included in the model

Reaction	Electron impact reaction type	Label
$e + SF_6 \rightarrow SF_6 + e$	Momentum transfer	1
$e + SF_6 \rightarrow SF_5 + F + e$	Dissociation	2
$e + SF_6 \rightarrow SF_6^-$	Electron attachment	3
$e + SF_6 \rightarrow SF_5^- + F$	Dissociative attachment	4
$e + SF_6 \rightarrow F^- + SF_5$	Dissociative attachment	5
$e + SF_6 \rightarrow SF_4^- + 2 F$	Dissociative attachment	6
$e + SF_6 \rightarrow SF_3^- + 3 F$	Dissociative attachment	7
$e + SF_6 \rightarrow SF_2^- + 4 F$	Dissociative attachment	8
$e + SF_6 \rightarrow SF_5^+ + F + 2 e$	Dissociative ionization	9
$e + SF_6 \rightarrow SF_3 + 3 F + e$	Dissociation	10
$e + SF_6 \rightarrow SF_4^+ + 2 F + 2 e$	Dissociative ionization	11
$e + SF_6 \rightarrow SF_3^+ + 3 F + 2 e$	Dissociative ionization	12
$e + SF_6 \rightarrow SF_2^+ + 2 F + F_2 + 2 e$	Dissociative ionization	13
$e + SF_6 \rightarrow SF^+ + 3 F + F_2 + 2 e$	Dissociative ionization	14
$e + SF_6 \rightarrow S^+ + 2 F + 2 F_2 + 2 e$	Dissociative ionization	15
$e + SF_6 \rightarrow F^+ + SF_4 + F + 2 e$	Dissociative ionization	16
$e + SF_5 \rightarrow SF_5 + e$	Momentum transfer	1
$e + SF_5 \rightarrow SF_4 + F + e$	Dissociation	17
$e + SF_5 \rightarrow SF_5^+ + 2 e$	Ionization	18
$e + SF_5 \rightarrow SF_4^+ + F + 2 e$	Dissociative ionization	19
$e + SF_4 \rightarrow SF_4 + e$	Momentum transfer	1
$e + SF_4 \rightarrow SF_3 + F + e$	Dissociation	20
$e + SF_4 \rightarrow SF_4^+ + 2 e$	Ionization	21
$e + SF_3 \rightarrow SF_3 + e$	Momentum transfer	1
$e + SF_3 \rightarrow SF_2 + F + e$	Dissociation	22
$e + SF_3 \rightarrow SF_3^+ + 2 e$	Ionization	23
$e + SF_2 \rightarrow SF_2 + e$	Momentum transfer	1
$e + SF_2 \rightarrow SF + F + e$	Dissociation	24
$e + SF_2 \rightarrow SF_2^+ + 2 e$	Ionization	25
$e + SF \rightarrow SF + e$	Momentum transfer	1
$e + SF \rightarrow S + F + e$	Dissociation	26
$e + SF \rightarrow SF^+ + 2 e$	Ionization	27
$e + S \rightarrow S + e$	Momentum transfer	28
$e + S \rightarrow S^+ + 2 e$	Ionization	29
$e + F \rightarrow F + e$	Momentum transfer	30
$e + F \rightarrow F^* + e$	Electronic excitation (12.70 eV; 12.99 eV)	31, 32
$e + F \rightarrow F^+ + 2 e$	Ionization	33
$e + F^* \rightarrow F^* + e$	Momentum transfer	30
$e + F^* \rightarrow F + e$	Quenching	34
$e + F^* \rightarrow F^+ + 2 e$	Ionization	35
$e + F_2 \rightarrow F_2 + e$	Momentum transfer	36
$e + F_2 \rightarrow F^- + F$	Dissociative attachment	37
$e + F_2 \rightarrow 2 F + e$	Dissociation	38
$e + F_2 \rightarrow F_2^+ + 2 e$	Ionization	39
$e + F_2^+ \rightarrow F_2^+ + e$	Momentum transfer	40

(Continues)

TABLE 2 (Continued)

Reaction	Electron impact reaction type	Label
$e + F_2^+ \rightarrow F + F$	Dissociative recombination	41
$e + O_2 \rightarrow O_2 + e$	Momentum transfer	42
$e + O_2 \rightarrow O^- + O$	Dissociative attachment	43
$e + O_2 \rightarrow 2 O + e$	Dissociation	44
$e + O_2 \rightarrow O^* + O + e$	Dissociation	45
$e + O_2 \rightarrow O_2^+ + 2 e$	Ionization	46
$e + O_2 \rightarrow O + O^+ + 2 e$	Dissociative ionization	47
$e + O_2^+ \rightarrow O + O$	Dissociative recombination	48
$e + O \rightarrow O + e$	Momentum transfer	49
$e + O \rightarrow O^* + e$	Electronic excitation (1.97 eV; 4.19 eV)	50, 51
$e + O \rightarrow O^+ + 2 e$	Ionization	52
$e + O^* \rightarrow O + e$	Quenching	53
$e + O^* \rightarrow O^+ + 2 e$	Ionization	54

Reactions with SF₆ are taken from refs.^[26–28] and those with O₂ from refs.^[29–31]

the formula to obtain the rate coefficient, but we lowered the coefficient with one order of magnitude, as suggested in the paper describing this method.^[25]

3 | RESULTS AND DISCUSSION

3.1 | Effect of wafer temperature on the etch rate at low or no oxygen content

The silicon wafers were etched under the following operating conditions: 5 Pa chamber pressure, 1000 W coil power operated at 13.56 MHz, a total gas flow rate of 200 sccm pure SF₆, without bias and with bias voltages of –50 and –100 V, also operated at 13.56 MHz. The applied bias voltages of –50 and –100 V correspond to bias powers of 60 and 150 W, respectively. The measured etch rates obtained for different wafer temperatures are plotted in Figure 3.

The etch rates clearly increase when the wafer becomes colder up till a temperature of about –110 °C. After this critical temperature the SF₆ gas starts to condense on the wafer (i.e., it forms a liquid layer on the surface), effectively limiting the etch rate to a value close to zero (i.e., denoted in Figure 3 as “X”). This phenomenon, where the etch rate abruptly drops to a value near zero, either caused by a too low wafer temperature or by too much oxygen in the SF₆/O₂ mixture, is called the “etch stop” phenomenon.^[32]

The reason for the increasing etch rates as a function of wafer temperature going from 20 to –100 °C is the active cooling of the gas near the wafer surface by the wafer, yielding a higher density of species in this area, for a fixed reactor pressure, following the ideal gas law. As a result, the higher flux toward the wafer of reactive species like the F

TABLE 3 Reactions between the heavy particles included in the model

Reaction type	Rate coefficient ($\text{cm}^3 \text{s}^{-1}$)
Chemical reactions	
$\text{SF} + \text{SF} \rightarrow \text{S} + \text{SF}_2$	2.50×10^{-11}
$\text{SF}_3 + \text{SF}_3 \rightarrow \text{SF}_2 + \text{SF}_4$	2.50×10^{-11}
$\text{SF}_5 + \text{SF}_5 \rightarrow \text{SF}_4 + \text{SF}_6$	2.50×10^{-11}
$\text{F}_2 + \text{SF}_5 \rightarrow \text{SF}_6 + \text{F}$	$2.62 \times 10^{-12} \exp(-2440(\text{K})/\text{T}(\text{K}))$
$\text{F}_2 + \text{SF}_4 \rightarrow \text{SF}_5 + \text{F}$	$2.62 \times 10^{-11} \exp(-7350(\text{K})/\text{T}(\text{K}))$
$\text{F}_2 + \text{SF}_3 \rightarrow \text{SF}_4 + \text{F}$	$2.62 \times 10^{-11} \exp(-7350(\text{K})/\text{T}(\text{K}))$
$\text{F}_2 + \text{SF}_2 \rightarrow \text{SF}_3 + \text{F}$	$2.62 \times 10^{-11} \exp(-7350(\text{K})/\text{T}(\text{K}))$
$\text{F}_2 + \text{SF} \rightarrow \text{SF}_2 + \text{F}$	$2.62 \times 10^{-11} \exp(-7350(\text{K})/\text{T}(\text{K}))$
$\text{F}_2 + \text{S} \rightarrow \text{F} + \text{SF}$	$2.91 \times 10^{-11} \exp(-7350(\text{K})/\text{T}(\text{K}))$
$\text{SF}_5 + \text{O} \rightarrow \text{SOF}_4 + \text{F}$	1.00×10^{-12}
$\text{SF}_4 + \text{O} \rightarrow \text{SOF}_3 + \text{F}$	$1.00 \times 10^{-12\text{a}}$
$\text{SF}_3 + \text{O} \rightarrow \text{SOF}_2 + \text{F}$	1.00×10^{-12}
$\text{SF}_2 + \text{O} \rightarrow \text{SOF} + \text{F}$	$1.00 \times 10^{-12\text{a}}$
$\text{SF} + \text{O} \rightarrow \text{SOF}$	1.00×10^{-10}
$\text{SOF}_4 + \text{O} \rightarrow \text{SO}_2\text{F}_2 + \text{F} + \text{F}$	$1.00 \times 10^{-10\text{a}}$
$\text{SOF}_3 + \text{O} \rightarrow \text{SO}_2\text{F}_2 + \text{F}$	1.00×10^{-10}
$\text{SOF}_2 + \text{O} \rightarrow \text{SO}_2\text{F}_2$	1.00×10^{-15}
$\text{SOF} + \text{O} \rightarrow \text{SO}_2 + \text{F}$	$1.00 \times 10^{-10\text{a}}$
$\text{SO}_2\text{F}_2 + \text{O} \rightarrow \text{SOF}_2 + \text{O}_2$	1.00×10^{-12}
$\text{SOF}_3 + \text{F}_2 \rightarrow \text{SOF}_4 + \text{F}$	1.00×10^{-11}
$\text{SOF}_2 + \text{F}_2 \rightarrow \text{SOF}_3 + \text{F}$	1.00×10^{-11}
$\text{SOF} + \text{F}_2 \rightarrow \text{SOF}_2 + \text{F}$	$1.00 \times 10^{-11\text{a}}$
$\text{SO}_2 + \text{F}_2 \rightarrow \text{SOF} + \text{O} + \text{F}$	$1.00 \times 10^{-11\text{a}}$
Electron detachment reactions ($X = \text{F}, \text{F}_2,$ or SF_{0-6})	
$\text{F}^- + X \rightarrow \text{F} + X + e$	5.27×10^{-10}
$\text{SF}_2^- + X \rightarrow \text{SF}_2 + X + e$	2.92×10^{-10}
$\text{SF}_3^- + X \rightarrow \text{SF}_3 + X + e$	2.92×10^{-10}
$\text{SF}_4^- + X \rightarrow \text{SF}_4 + X + e$	2.92×10^{-10}
$\text{SF}_5^- + X \rightarrow \text{SF}_5 + X + e$	2.92×10^{-10}
$\text{SF}_6^- + X \rightarrow \text{SF}_6 + X + e$	2.92×10^{-10}
Ion-ion neutralization reactions	
$\text{F}^- + \text{F}_2^+ \rightarrow \text{F} + \text{F}_2$	6.66×10^{-8}
$\text{F}^- + \text{F}^+ \rightarrow \text{F} + \text{F}$	7.69×10^{-9}
$\text{F}^- + \text{S}^+ \rightarrow \text{F} + \text{S}$	6.86×10^{-9}
$\text{F}^- + \text{SF}^+ \rightarrow \text{F} + \text{SF}$	6.37×10^{-8}
$\text{F}^- + \text{SF}_2^+ \rightarrow \text{F} + \text{SF}_2$	6.13×10^{-8}
$\text{F}^- + \text{SF}_3^+ \rightarrow \text{F} + \text{SF}_3$	5.99×10^{-8}
$\text{F}^- + \text{SF}_4^+ \rightarrow \text{F} + \text{SF}_4$	5.89×10^{-8}
$\text{F}^- + \text{SF}_5^+ \rightarrow \text{F} + \text{SF}_5$	5.83×10^{-8}
$\text{F}^- + \text{O}_2^+ \rightarrow \text{F} + \text{O}_2$	6.86×10^{-8}
$\text{F}^- + \text{O}^+ \rightarrow \text{F} + \text{O}$	8.04×10^{-9}
$\text{O}^- + \text{F}_2^+ \rightarrow \text{O} + \text{F}_2$	7.31×10^{-8}
$\text{O}^- + \text{F}^+ \rightarrow \text{O} + \text{F}$	8.32×10^{-8}
$\text{O}^- + \text{S}^+ \rightarrow \text{O} + \text{S}$	7.51×10^{-9}
$\text{O}^- + \text{SF}^+ \rightarrow \text{O} + \text{SF}$	7.03×10^{-8}

(Continues)

TABLE 3 (Continued)

Reaction type	Rate coefficient ($\text{cm}^3 \text{s}^{-1}$)
$\text{O}^- + \text{SF}_2^+ \rightarrow \text{O} + \text{SF}_2$	6.80×10^{-8}
$\text{O}^- + \text{SF}_3^+ \rightarrow \text{O} + \text{SF}_3$	6.66×10^{-8}
$\text{O}^- + \text{SF}_4^+ \rightarrow \text{O} + \text{SF}_4$	6.57×10^{-8}
$\text{O}^- + \text{SF}_5^+ \rightarrow \text{O} + \text{SF}_5$	6.51×10^{-8}
$\text{O}^- + \text{O}_2^+ \rightarrow \text{O} + \text{O}_2$	7.51×10^{-8}
$\text{O}^- + \text{O}^+ \rightarrow \text{O} + \text{O}$	8.67×10^{-9}
$\text{SF}_2^- + \text{F}_2^+ \rightarrow \text{SF}_2 + \text{F}_2$	3.83×10^{-8}
$\text{SF}_2^- + \text{F}^+ \rightarrow \text{SF}_2 + \text{F}$	4.91×10^{-8}
$\text{SF}_2^- + \text{S}^+ \rightarrow \text{SF}_2 + \text{S}$	4.05×10^{-8}
$\text{SF}_2^- + \text{SF}^+ \rightarrow \text{SF}_2 + \text{SF}$	3.50×10^{-8}
$\text{SF}_2^- + \text{SF}_2^+ \rightarrow \text{SF}_2 + \text{SF}_2$	3.21×10^{-8}
$\text{SF}_2^- + \text{SF}_3^+ \rightarrow \text{SF}_2 + \text{SF}_3$	3.03×10^{-8}
$\text{SF}_2^- + \text{SF}_4^+ \rightarrow \text{SF}_2 + \text{SF}_4$	2.91×10^{-8}
$\text{SF}_2^- + \text{SF}_5^+ \rightarrow \text{SF}_2 + \text{SF}_5$	2.83×10^{-8}
$\text{SF}_2^- + \text{O}_2^+ \rightarrow \text{SF}_2 + \text{O}_2$	4.05×10^{-8}
$\text{SF}_2^- + \text{O}^+ \rightarrow \text{SF}_2 + \text{O}$	5.26×10^{-8}
$\text{SF}_3^- + \text{F}_2^+ \rightarrow \text{SF}_3 + \text{F}_2$	3.88×10^{-8}
$\text{SF}_3^- + \text{F}^+ \rightarrow \text{SF}_3 + \text{F}$	5.06×10^{-8}
$\text{SF}_3^- + \text{S}^+ \rightarrow \text{SF}_3 + \text{S}$	4.13×10^{-8}
$\text{SF}_3^- + \text{SF}^+ \rightarrow \text{SF}_3 + \text{SF}$	3.52×10^{-8}
$\text{SF}_3^- + \text{SF}_2^+ \rightarrow \text{SF}_3 + \text{SF}_2$	3.20×10^{-8}
$\text{SF}_3^- + \text{SF}_3^+ \rightarrow \text{SF}_3 + \text{SF}_3$	3.00×10^{-8}
$\text{SF}_3^- + \text{SF}_4^+ \rightarrow \text{SF}_3 + \text{SF}_4$	2.87×10^{-8}
$\text{SF}_3^- + \text{SF}_5^+ \rightarrow \text{SF}_3 + \text{SF}_5$	2.77×10^{-8}
$\text{SF}_3^- + \text{O}_2^+ \rightarrow \text{SF}_3 + \text{O}_2$	4.13×10^{-8}
$\text{SF}_3^- + \text{O}^+ \rightarrow \text{SF}_3 + \text{O}$	5.44×10^{-8}
$\text{SF}_4^- + \text{F}_2^+ \rightarrow \text{SF}_4 + \text{F}_2$	4.05×10^{-8}
$\text{SF}_4^- + \text{F}^+ \rightarrow \text{SF}_4 + \text{F}$	5.34×10^{-8}
$\text{SF}_4^- + \text{S}^+ \rightarrow \text{SF}_4 + \text{S}$	4.32×10^{-8}
$\text{SF}_4^- + \text{SF}^+ \rightarrow \text{SF}_4 + \text{SF}$	3.65×10^{-8}
$\text{SF}_4^- + \text{SF}_2^+ \rightarrow \text{SF}_4 + \text{SF}_2$	3.29×10^{-8}
$\text{SF}_4^- + \text{SF}_3^+ \rightarrow \text{SF}_4 + \text{SF}_3$	3.07×10^{-8}
$\text{SF}_4^- + \text{SF}_4^+ \rightarrow \text{SF}_4 + \text{SF}_4$	2.92×10^{-8}
$\text{SF}_4^- + \text{SF}_5^+ \rightarrow \text{SF}_4 + \text{SF}_5$	2.81×10^{-8}
$\text{SF}_4^- + \text{O}_2^+ \rightarrow \text{SF}_4 + \text{O}_2$	4.32×10^{-8}
$\text{SF}_4^- + \text{O}^+ \rightarrow \text{SF}_4 + \text{O}$	5.75×10^{-8}
$\text{SF}_5^- + \text{F}_2^+ \rightarrow \text{SF}_5 + \text{F}_2$	4.37×10^{-8}
$\text{SF}_5^- + \text{F}^+ \rightarrow \text{SF}_5 + \text{F}$	5.82×10^{-8}
$\text{SF}_5^- + \text{S}^+ \rightarrow \text{SF}_5 + \text{S}$	4.68×10^{-8}
$\text{SF}_5^- + \text{SF}^+ \rightarrow \text{SF}_5 + \text{SF}$	3.92×10^{-8}
$\text{SF}_5^- + \text{SF}_2^+ \rightarrow \text{SF}_5 + \text{SF}_2$	3.52×10^{-8}
$\text{SF}_5^- + \text{SF}_3^+ \rightarrow \text{SF}_5 + \text{SF}_3$	3.27×10^{-8}
$\text{SF}_5^- + \text{SF}_4^+ \rightarrow \text{SF}_5 + \text{SF}_4$	3.10×10^{-8}
$\text{SF}_5^- + \text{SF}_5^+ \rightarrow \text{SF}_5 + \text{SF}_5$	2.97×10^{-8}
$\text{SF}_5^- + \text{O}_2^+ \rightarrow \text{SF}_5 + \text{O}_2$	4.68×10^{-8}

(Continues)

TABLE 3 (Continued)

Reaction type	Rate coefficient ($\text{cm}^3 \text{s}^{-1}$)
$\text{SF}_5^- + \text{O}^+ \rightarrow \text{SF}_5 + \text{O}$	6.28×10^{-8}
$\text{SF}_6^- + \text{F}_2^+ \rightarrow \text{SF}_6 + \text{F}_2$	5.09×10^{-8}
$\text{SF}_6^- + \text{F}^+ \rightarrow \text{SF}_6 + \text{F}$	6.81×10^{-8}
$\text{SF}_6^- + \text{S}^+ \rightarrow \text{SF}_6 + \text{S}$	5.45×10^{-8}
$\text{SF}_6^- + \text{SF}^+ \rightarrow \text{SF}_6 + \text{SF}$	4.55×10^{-8}
$\text{SF}_6^- + \text{SF}_2^+ \rightarrow \text{SF}_6 + \text{SF}_2$	4.06×10^{-8}
$\text{SF}_6^- + \text{SF}_3^+ \rightarrow \text{SF}_6 + \text{SF}_3$	3.76×10^{-8}
$\text{SF}_6^- + \text{SF}_4^+ \rightarrow \text{SF}_6 + \text{SF}_4$	3.55×10^{-8}
$\text{SF}_6^- + \text{SF}_5^+ \rightarrow \text{SF}_6 + \text{SF}_5$	3.39×10^{-8}
$\text{SF}_6^- + \text{O}_2^+ \rightarrow \text{SF}_6 + \text{O}_2$	5.45×10^{-8}
$\text{SF}_6^- + \text{O}^+ \rightarrow \text{SF}_6 + \text{O}$	7.36×10^{-8}

The rate coefficients for the chemical reactions and the electron detachment reactions are taken from references^[18,24,26–28] while the rate coefficients for the ion-ion neutralization reactions are adopted from refs.^[25]

^aThese reactions were estimated based on similar reactions from refs.^[18,24]

atoms entails a slightly higher etch rate. A similar effect was also observed and explained in our previous work.^[19] To illustrate this, we present the calculated total gas density profiles as well as the average gas temperature for both -100 and 20 °C wafers in Figure 4A,B, respectively.

It can thus be concluded that cooling the wafer has a beneficial effect on the etch rate, at least for very low or no oxygen content. However, as mentioned earlier, cooling of the wafer and the gas near its surface entails a higher gas density, and thus more gas phase collisions, which effectively reduces the total ion flux toward the wafer. The reason for this is that a denser gas is less diffusive, increasing the travel time for ions generated near the ICP source toward the wafer, hence increasing the chance for neutralization reactions to happen before the ions arrive at the wafer. In other words, when the wafer is cooled, the fluxes of reactive neutrals will become somewhat higher while the fluxes of ions will drop. This is confirmed by our simulations as presented in Figure 5, showing a slightly rising flux of F atoms and a slightly decreasing total ion flux as a function of decreasing wafer temperature. It also shows slightly higher ion fluxes and slightly lower F atom fluxes as a function of bias voltage. This is explained as follows: increasing the bias will also slightly heat the gas above the wafer, reversing this effect. Applying a bias thus will slightly decrease the F atom flux and increase the ion flux as well as sputter yield. The overall etch process will become more anisotropic in general when a bias is applied.

However, the gas heating near the wafer due to the bias power is limited, not creating a large enough discrepancy between actual etch rates when the wafer temperature is low enough (i.e., 40 °C or lower) as is clear from Figure 3.

On a side note, we would also like to point out that the calculated ion energy and angular distributions (IED and IAD) of the ions arriving at the wafer did not vary for different wafer temperatures. Under the investigated conditions, the sheath is always collisionless and not influenced by wafer temperature. As a result, the IED and IAD are not significantly affected by the wafer temperature, unlike the ion flux which decreases with colder wafer temperatures.

The etch rate thus becomes slightly less anisotropic upon cooling the wafer due to less physical sputtering and more isotropic chemical etching. Note that this is only true at very low or no oxygen content, where no sidewall passivation occurs. This explains why the measured etch rates without bias and with bias tend to become similar at low wafer temperatures, as shown in Figure 3. Indeed, introduction of a bias will slightly heat the gas in the area near the wafer, resulting in less F atoms and more ions arriving at the wafer. However, from Figure 5 it is clear that the flux of F atoms increases by about 6% in the temperature range of 20 to -100 °C while the ion flux decreases with a similar percentage. Since the F atom flux is roughly 100 times higher than the total ion flux, and since the F atoms are very reactive toward the silicon wafer, it can be concluded that in this

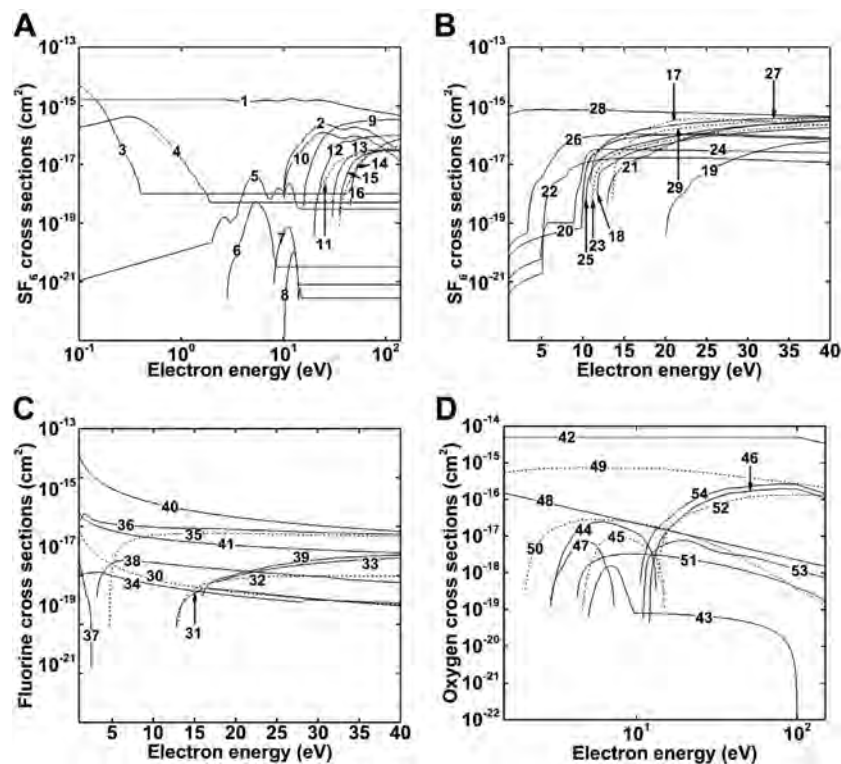


FIGURE 2 Cross sections of the electron impact reactions included in the model, divided over several plots for clarity. The labels correspond to the reactions shown in Table 2. Some X-axis scales are logarithmic instead of linear for clarity

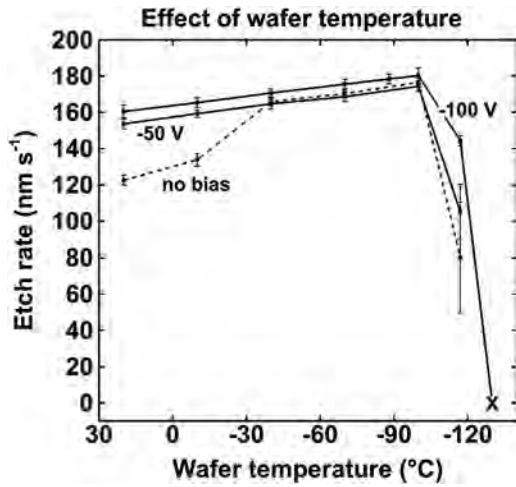


FIGURE 3 Measured etch rates for pure SF₆ plasma without bias and with bias voltages of -50 and -100 V, as a function of wafer temperature. At “X” the etch rate could not be measured properly, which refers to a situation where the gas condenses on the wafer surface, inhibiting further etching (i.e., etch stop)

case (i.e., without O₂) the overall etch rate is defined mainly by the rate of chemical etching by F atoms.

3.2 | Combined effects of wafer temperature and oxygen content on the etch rate without bias voltage

The same conditions as mentioned in the previous section were applied to etch the wafers at different wafer temperatures and

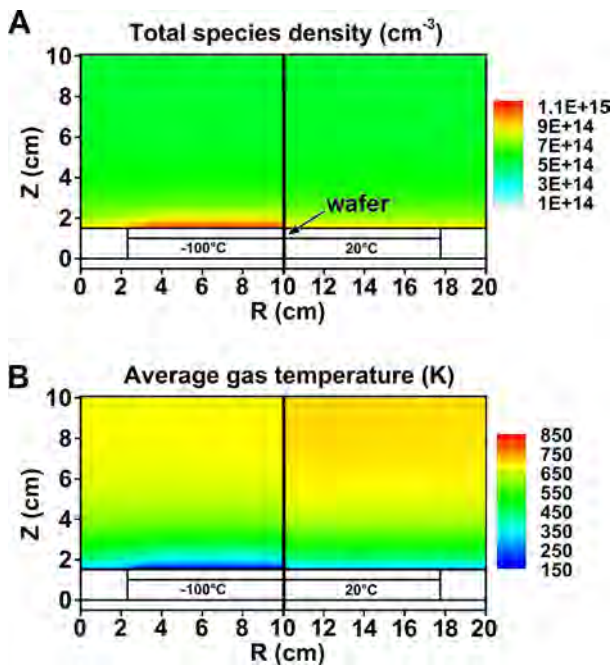


FIGURE 4 Calculated total species density (A) and average gas temperature (B) in the area near the wafer for a -100 °C wafer temperature (left) and a 20 °C wafer temperature (right). Please note that this is only a partial section of the computational grid involving the complete reactor

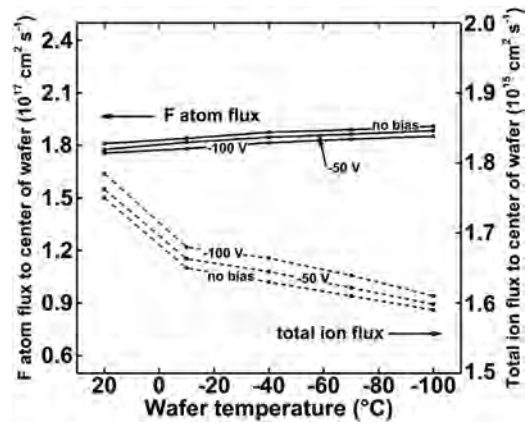


FIGURE 5 Calculated F atom flux and total ion flux toward the center of the wafer as a function of wafer temperature, for the conditions mentioned in the beginning of Section 3.1

for different SF₆/O₂ ratios in the mixture, without using a bias voltage and keeping the total gas flow rate fixed at 200 sccm. The measured etch rates are presented in Figure 6.

First, we should note from Figure 6 that at very low oxygen content (i.e., 0-3%), the etch rate increases upon cooling the wafer, as was explained in the previous section.

It is also clear that, for all wafer temperatures, the etch rate is fairly constant at low oxygen content, but above a critical oxygen fraction it drops abruptly to a value near zero. When the O₂ percentage is higher than this critical value, the process changes from an etching regime to the formation of an oxifluoride passivation layer, what we call the “etch stop” phenomenon, as mentioned earlier. The oxidation threshold had also been studied and reported by Tillocher et al. who analyzed the plasma species by mass spectrometry and by increasing the oxygen flow.^[33]

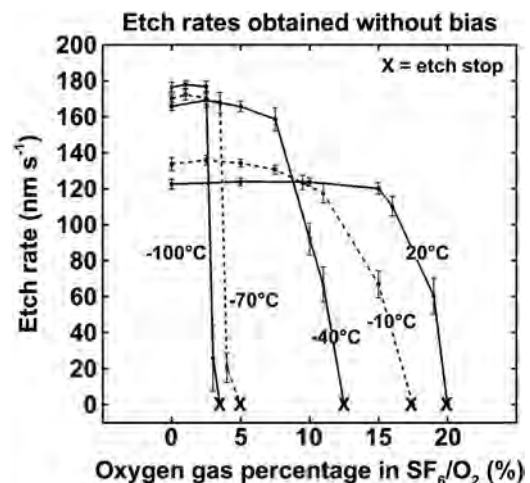


FIGURE 6 Measured etch rates without bias voltage, for different wafer temperatures and different oxygen contents in the SF₆/O₂ gas mixture. The other operating conditions are the same as mentioned in the beginning of Section 3.1

The abrupt transition from an etching regime to a passivation regime indicates that the overall etch rate is determined by at least two processes that are in competition, more specifically (i) etching of silicon mainly by F atoms, and (ii) passivation layer formation mainly by O atoms. Sputtering by ions plays a minor role in this case, as there is no bias voltage applied. The overall etch rate is thus mainly determined by the ratio between the F flux and O flux toward the wafer.

Both the calculated F and O fluxes are plotted in Figure 7A, while their ratio is shown in Figure 7B, for different wafer temperatures and as a function of O₂ percentage.

As is clear from Figure 7A, the calculated fluxes of the F atoms decrease while the fluxes of the O atoms increase as a function of O₂ percentage, which is expected. Also, the fluxes toward the wafer are always higher when the wafer is colder, as was explained in the previous section. Moreover, the flux of F atoms is at least 80 times higher than the flux of O atoms, as can be concluded from their ratio shown in Figure 7B. Finally, the F atom flux toward the wafer increases more slowly upon decreasing temperature than the O atom flux, which results in a drop of the F/O flux ratio with decreasing wafer temperature (see Figure 7B). Thus, cooling of the wafer changes the ratio between F and O fluxes in favor of passivation layer formation, regardless of the SF₆/O₂ gas mixing ratio. However, we may not conclude that passivation layer formation occurs more rapidly at lower wafer temperatures simply because there is a shift in F/O flux ratio in favor of passivation. Indeed, if the ratio between the F and O fluxes would be the only factor defining the overall etch rate, we would find the critical point where etch stop occurs always for the same F/O flux ratio, regardless of wafer temperature. This is not the case, as is clear from Figure 8, showing the critical F/O ratios where etch stop first occurs, as a function of wafer temperature.

It is apparent from Figure 8 that this critical F/O ratio increases with colder wafer temperature nearly linearly, at least for the investigated temperature range. Undoubtedly, Figure 8 indicates that the etch rate is not solely dependent on the F, O fluxes arriving at the wafer, but that there is a change in the etching surface reaction mechanism with temperature. Indeed, a lower wafer temperature seems to favor passivation layer formation, as it yields a higher critical F/O flux for full etch stop, which might be due to enhanced surface sticking of O. Most likely, the actual sticking probabilities do not change significantly in the investigated temperature range, as was concluded in our previous work involving an atomistic calculation technique (Molecular Dynamics) to predict sticking coefficients of fluorine on silicon as a function of wafer temperature.^[34] This combined information suggests that the formation of the passivation layer is most probably

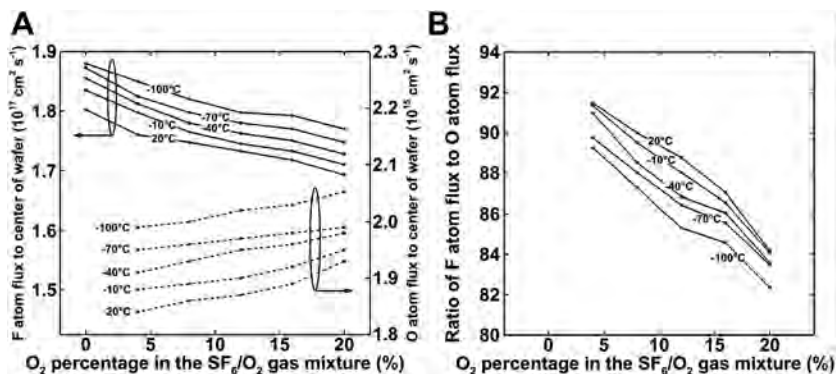


FIGURE 7 (A) Calculated F and O fluxes and (B) calculated F/O flux ratio toward the center of the wafer for different wafer temperatures as a function of O₂ gas fraction, at the same conditions as mentioned in the beginning of Section 3.1

influenced by the behavior of physisorbed species which have longer residence times on the surface at colder wafer temperatures. The actual mechanism of how the passivation layer is formed as a function of wafer temperature must be investigated with atomistic simulation techniques and is beyond the scope of the current work.

3.3 | Additional effects of bias voltage in combination with wafer temperature and oxygen content

When a sufficiently strong bias voltage is applied, sputtering by ions also becomes an important factor affecting the overall etch rate, in addition to the fluxes of F and O atoms and the wafer temperature. Figure 9A,B show the etch rates measured for different O₂ fractions and wafer temperatures, at bias voltages of -50 and -100 V, respectively.

Similar to the case where no bias is applied, the etch rates all decrease with increasing O₂ fraction, as expected. However, the etch rates no longer decrease abruptly at a critical O₂ fraction, but they drop consistently with rising O₂

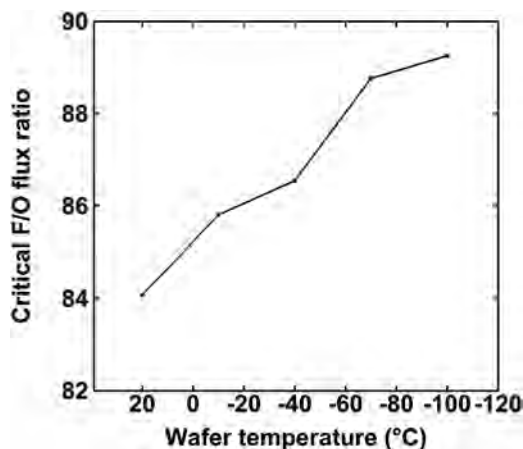


FIGURE 8 Calculated critical ratio of F atom flux over O atom flux toward the wafer, where full etch stop starts to occur, for different wafer temperatures, as can be deduced from Figures 6 and 7Bgr8

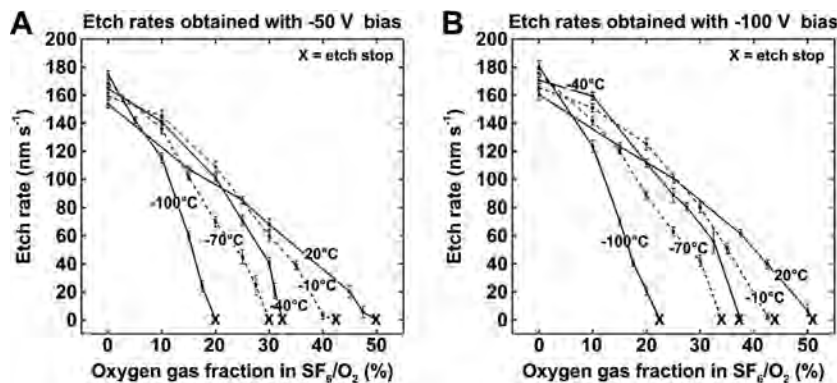


FIGURE 9 Measured etch rates obtained with a bias voltage of -50 V (A) and -100 V (B), for different wafer temperatures as a function of the O_2 fraction in the mixture. The other operating conditions are the same as mentioned in the beginning of Section 3.1

percentage. This suggests that the growth of a passivation layer is thwarted by ion bombardment, through removal of the passivation layer at the bottom of the trench or hole during etching. As a result, the etch rate is now mainly dependent on the number of F atoms that reach the wafer surface, which gradually decreases with O_2 content, and on the amount of sputtering. As is clear from Figure 10, the flux of F atoms does indeed decrease as a function of O_2 content as mentioned earlier and the same applies to the total ion flux. The most abundant ions under the investigated conditions are always SF_5^+ , making up 89% of the total ion flux at 0% O_2 and 48% at 20% O_2 . As a result, the total ion flux changes along with the density of SF_5^+ . The most important processes to create SF_5^+ ions are electron impact dissociative ionization of SF_6 (Table 2; label 9; threshold = 15.9 eV) and electron impact ionization of SF_5 (Table 2; label 18; threshold = 11.8 eV). Both processes are almost equally important. The second most abundant ion is O_2^+ (except for the case without O_2), which only has one significant path for creation: electron impact ionization of O_2 (Table 2; label 46; threshold = 12.1 eV). As a result, the formation of positive ions is diminished with increasing O_2 gas percentage, as is clear from Figure 10.

The etch rate thus decreases fairly linearly with O_2 fraction, since both the F atom and total ion fluxes also show a drop as a function of O_2 percentage. As explained in Section 3.1, the F atom flux increases with decreasing wafer temperature due to the higher gas density, while the ion density decreases slightly. The latter is due to the less diffusive character of the denser gas, imposing a longer travel time for the ions from source to wafer, resulting in a higher chance for ions to become neutralized before reaching the wafer surface, as explained above. It must be noted that this trend (i.e., where the ion flux decreases with colder wafer temperature) can be different for different reactor geometries and is strongly influenced by the distance between plasma source (i.e., ICP coil(s)) and wafer. If the wafer is placed near the plasma source, the loss of ions diffusing toward the wafer

will be less pronounced and a different trend can be observed, for example, a constant ion flux for different wafer temperatures.

Even with significant ion sputtering, it is clear that a lower wafer temperature enhances the formation of a passivation layer. For example, from Figure 9A we can conclude that the etch stop occurs above a critical value of about 50% O_2 , when the wafer is 20 °C. At -100 °C, passivation layer formation becomes dominant already at 20% O_2 . When the bias voltage is stronger, and thus sputtering is more pronounced, it will be easier to remove the passivation layer, as can be concluded when comparing Figure 9A,B. Indeed at -100 V bias voltage and for similar

temperatures, etch stop occurs when the O_2 fraction is 2-3% higher compared to the cases at -50 V.

There are other interesting conclusions that can be drawn when comparing the cases with and without bias for a given wafer temperature. For clarity and ease of explanation, these are presented together in Figure 11A-E.

Figure 11A clearly illustrates the transformation from an abrupt etch stop regime without bias to an almost linear decrease in etch rate as a function of O_2 percentage when sputtering by ions is significant, as explained above. It is interesting to note that in some cases the etch rate without bias can, in fact, be slightly higher than with a small bias voltage applied (e.g., see Figure 11A; at 16% O_2 without bias and with -50 V bias). As mentioned in Section 3.1, the introduction of a bias voltage causes some additional heating of the gas located near the wafer. A higher gas temperature will decrease the flux of F atoms and increase the flux of ions, but the decrease in F atom flux is much more significant, resulting in an overall decrease of the etch rate, especially

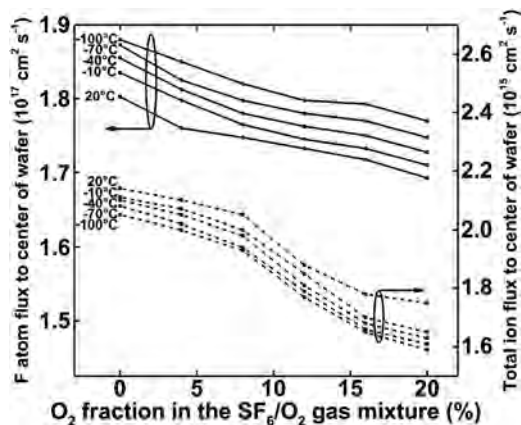


FIGURE 10 Calculated F atom flux (solid lines) and total ion flux (dashed lines) toward the center of the wafer as a function of oxygen fraction and for various wafer temperatures. The conditions are the same as mentioned in the beginning of Section 3.1, without an applied bias

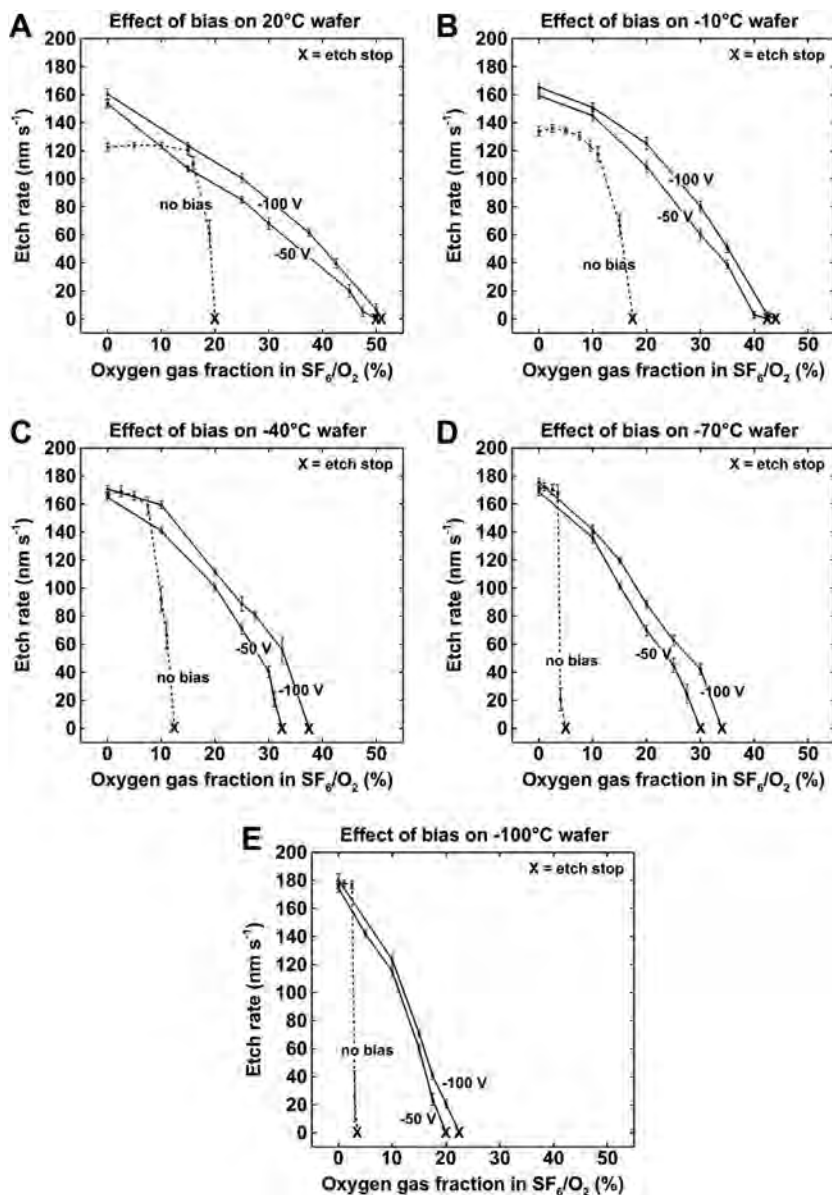


FIGURE 11 Measured etch rates obtained without bias, and with a bias voltage of -50 and -100 V, as a function of O_2 percentage in the mixture, for wafer temperatures of (A) 20°C , (B) -10°C , (C) -40°C , (D) -70°C , and (E) -100°C . The other operating conditions are the same as mentioned in the beginning of Section 3.1

under conditions of low O_2 content and when passivation layer formation is nearly absent.

The collective data presented in Figure 11A-E allow the reader to find proper operating conditions for successful anisotropic (cryo)etching. Indeed, in practice, anisotropic etching always requires a sufficiently strong bias voltage, and the results without bias shown here in fact refer to the etch rates at the sidewalls of the trench or hole, as ion bombardment is negligible here. For example, if we cool the wafer to -100°C (see Figure 11E), an O_2 percentage of 10% and a bias voltage of -100 V are suitable conditions for anisotropic etching, as the etch rate will be about 120 nm s^{-1} , while at the same time successful etch stop (or passivation

layer formation) will occur on the sidewalls (referring to the etch rate obtained without bias, which is virtually equal to zero).

It can be concluded that the introduction of a bias voltage will greatly influence the etch rate in such a manner that passivation layer formation is efficiently counteracted. The stronger the bias voltage, the lower the temperature or the more O_2 percentage is needed to create a passivation layer, although it must be noted that the difference between a bias voltage of -50 and -100 V is not very significant, especially at low wafer temperature. It is mainly the difference between a small bias voltage and no bias that is very significant. It is clear that adjusting the O_2 gas fraction, wafer temperature and bias voltage together allows proper conditions for successful anisotropic etching.

4 | CONCLUSION

We performed both experimental and numerical investigations on the etching of silicon with an SF₆/O₂ ICP, to elucidate the effects of the SF₆/O₂ gas ratio and the wafer temperature in the range -100 to 20°C on the etch process. At very low or no oxygen content, the etch rate slightly increases with decreasing wafer temperature due to additional cooling of the gas near the wafer, which results in a somewhat higher gas density. This in turn results in a slightly higher flux of F atoms but a somewhat lower total ion flux due to an increased chance for neutralization to occur before the ions arrive at the wafer. The etch process thus becomes a bit faster at cryogenic and oxygen-poor conditions, but also less anisotropic. However, below -110°C , the etch rate suddenly drops to virtually zero, when the gas starts to condense on the wafer.

At oxygen-rich conditions the formation of a passivation layer is enhanced at lower wafer temperatures, resulting in a lowering of the etch rate, which is in contrast to the slightly rising etch rate upon decreasing wafer temperature at low or no oxygen content. Our results indicate that the enhanced formation of the passivation layer at lower wafer temperatures is due to the lower ratio of F atom flux to O atom flux at lower wafer temperature, but this effect alone is not sufficient to explain the trend. Therefore, we expect that at low wafer temperatures the sticking of O atoms will be more pronounced, most probably due to physisorption, which is

in line with our previous MD calculations for the sticking of F atoms on Si.^[33]

Finally, our measurements show that the shift from an etching regime toward a passivation regime, and the degree of anisotropy during etching can be controlled by the amount of ion sputtering, because a stronger bias voltage will more efficiently remove the passivation layer. The reader can find suitable operating conditions for successful anisotropic etching from our collective results presented in the paper.

ACKNOWLEDGMENTS

The Fund for Scientific Research Flanders (FWO; grant no. 0880.212.840) is acknowledged for financial support of this work. The work was carried out in part using the Turing HPC infrastructure at the CalcUA core facility of the Universiteit Antwerpen, a division of the Flemish Supercomputer Center VSC, funded by the Hercules Foundation, the Flemish Government (department EWI), and the University of Antwerp. Also, we are very grateful to Mark Kushner for providing the HPEM computer code.

REFERENCES

- [1] M. McCoy, *Chem. Eng. News* **2000**, 78, 17.
- [2] L. Zhang, J. F. De Marneffe, F. Leroy, P. Lefauchaux, T. Tillocher, R. Dussart, K. Maekawa, K. Yatsuda, C. Dussarat, A. Goodyear, M. Cooke, S. De Gendt, M. Baklanov, *J. Phys. D: Appl. Phys.* **2016**, 49, 175203.
- [3] F. Leroy, L. Zhang, T. Tillocher, K. Yatsuda, K. Maekawa, E. Nishimura, P. Lefauchaux, J. F. De Marneffe, M. Baklanov, R. Dussart, *J. Phys. D: Appl. Phys.* **2015**, 48, 435202.
- [4] S. Tachi, K. Tsujimoto, S. Okudaira, *Appl. Phys. Lett.* **1988**, 52, 616.
- [5] R. Dussart, M. Boufnichel, G. Marcos, P. Lefauchaux, A. Basillais, R. Benoit, T. Tillocher, X. Mellhaoui, H. Estrade-Schwarzkopf, P. Ranson, *J. Micromech. Microeng.* **2004**, 14, 190.
- [6] R. Dussart, T. Tillocher, P. Lefauchaux, M. Boufnichel, *J. Phys. D: Appl. Phys.* **2014**, 47, 123001.
- [7] R. d'Agostino, D. Flamm, *J. Appl. Phys.* **1981**, 52, 162.
- [8] C. Mogab, A. Adams, D. L. Flamm, *J. Appl. Phys.* **1978**, 45, 3796.
- [9] J. Bartha, J. Greschner, M. Puech, P. Maquin, *Microelectron. Eng.* **1995**, 27, 453.
- [10] C. D'Emic, K. Chan, J. Blum, *J. Vac. Sci. Technol. B* **1992**, 10, 1105.
- [11] A. Campo, C. Cardinaud, G. Turban, *J. Vac. Sci. Technol. B* **1995**, 13, 235.
- [12] M. Reiche, U. Gösele, M. Wiegand, *Cryst. Res. Technol.* **2000**, 3, 807.
- [13] G. Craciun, M. Blauw, E. Van der Drift, P. Sarro, P. French, *J. Micromech. Microeng.* **2002**, 12, 390.
- [14] R. Dussart, M. Boufnichel, G. Marcos, P. Lefauchaux, A. Basillais, R. Benoit, P. Ranson, *J. Micromech. Microeng.* **2003**, 14, 190.
- [15] M. A. Blauw, E. van der Drift, G. Marcos, A. Rhallabi, *J. Appl. Phys.* **2003**, 94, 6311.
- [16] G. Marcos, A. Rhallabi, P. Ranson, *J. Vac. Sci. Technol. B* **2003**, 21, 87.
- [17] A. Pateau, A. Rhallabi, M. Fernandez, M. Boufnichel, F. Roqueta, *J. Vac. Sci. Technol. A* **2013**, 32, 021303.
- [18] F. Hamaoka, T. Yagisawa, T. Makabe, *IEEE Trans. On Plasma Sci.* **2007**, 35, 1350.
- [19] S. Tinck, T. Tillocher, R. Dussart, A. Bogaerts, *J. Phys. D: Appl. Phys.* **2015**, 48, 155204.
- [20] K. Ryan, I. Plumb, *Plasma Chem. Plasma Proc.* **1990**, 10, 207.
- [21] H. Anderson, J. Merson, R. Light, *IEEE Trans.* **1986**, 14, 156.
- [22] M. Boufnichel, S. Aachboun, P. Lefauchaux, P. Ranson, *J. Vac. Sci. Technol. B* **2003**, 21, 267.
- [23] M. Kushner, *J. Phys. D: Appl. Phys.* **2009**, 42, 194013.
- [24] S. Rauf, W. Dauksher, S. Clemens, K. Smith, *J. Vac. Sci. Technol. A* **2002**, 20, 1177.
- [25] N. Shuman, J. Wiens, T. Miller, A. Viggiano, *J. Chem. Phys.* **2014**, 140, 224309.
- [26] L. Christophorou, J. Olthoff, *J. Phys. Chem. Ref. Data* **2000**, 29, 267.
- [27] R. Rejoub, D. Sieglaff, B. Lindsay, R. Stebbings, *J. Phys. B: At. Mol. Opt. Phys.* **2001**, 34, 1289.
- [28] M. Mao, Y. N. Wang, A. Bogaerts, *J. Phys. D: Appl. Phys.* **2011**, 44, 435202.
- [29] T. Sommerer, M. Kushner, *J. Appl. Phys.* **1992**, 71, 1654.
- [30] C. Hsu, M. Nierode, J. Coburn, D. Graves, *J. Phys. D: Appl. Phys.* **2006**, 39, 3272.
- [31] S. Rauf, M. Kushner, *J. Appl. Phys.* **1997**, 82, 2805.
- [32] S. Tinck, D. Shamiryman, A. Bogaerts, *Plasma Process Polym.* **2011**, 8, 490.
- [33] T. Tillocher, R. Dussart, X. Mellhaoui, P. Lefauchaux, N. Mekkakia Maaza, P. Ranson, M. Boufnichel, L. Overzet, *J. Vac. Sci. Technol. A* **2006**, 24, 1073.
- [34] S. Tinck, E. C. Neyts, A. Bogaerts, *J. Phys. Chem. C* **2014**, 118, 30315.

How to cite this article: Tinck S, Tillocher T, Georgieva V, Dussart R, Neyts E, Bogaerts A. Concurrent effects of wafer temperature and oxygen fraction on cryogenic silicon etching with SF₆/O₂ plasmas. *Plasma Process Polym.* 2017;14:e1700018. <https://doi.org/10.1002/ppap.201700018>